MRS Advances (2024) 9:172–176
https://doi.org/10.1557/s43580-024-00765-9

ORIGINAL PAPER

Calcium-based promoter in Ni catalysts supported over nanostructured ZrO_2

V. Pérez-Madrigal[1] · D. Santiago-Salazar[1] · E. Ríos-Valdovinos[1] · E. Albiter[2] · M. A. Valenzuela[2] · F. Pola-Albores[1]

Received: 16 September 2023 / Accepted: 3 January 2024 / Published online: 17 January 2024

Abstract

This study investigates the impact of CaO addition on the catalytic performance of Ni/ZrO_2 materials for the dry reforming of methane. ZrO_2 supports were synthesized using the co-precipitation method, wherein CaO (2 and 10 wt%) was incorporated during the initial synthesis stage. Subsequently, these supports were impregnated with 15 wt% Ni. The catalysts were characterized by X-ray diffraction (XRD), wavelength dispersive X-ray fluorescence (WDXRF), temperature-programmed reduction (TPR), and Fourier transform infrared spectroscopy-DRIFTS. The catalytic evaluation was performed in a flow microreactor at 700 °C, using a feed gas ratio CH_4:CO_2 of 1. Introducing CaO enhanced the catalyst's basic sites, increasing catalytic activity. However, the catalytic performance did not correlate solely with the impregnated CaO percentages. The catalysts demonstrated varied performances, with the order of effectiveness observed as 10% CaO > 0% > 2% CaO. These findings underscore that catalysts with higher basicity also exhibited reduced carbon formation, a factor directly associated with catalyst deactivation.

Introduction

Among today's scientific challenges, global warming, largely attributed to greenhouse gases (GHGs), is a critical concern. Primary GHGs like methane (CH_4) and carbon dioxide (CO_2) have steered extensive investigations into their roles within various industrial processes. Specifically, the catalytic conversion of CO_2 and CH_4 presents a promising pathway for mitigating these gases. Notably, dry reforming of methane (DRM), as represented by the Eq. (1), holds substantial interest [1].

$$CH_4 + CO_2 \rightarrow 2CO + 2H_2 \quad \Delta H_r^{\circ} = 264\,\mathrm{kJ/mol}. \tag{1}$$

DRM offers a prospective strategy by transforming GHGs into syngas, a blend of carbon monoxide (CO) and hydrogen (H_2) [2]. This process becomes especially intriguing as a lower H_2/CO syngas ratio favors the synthesis of valuable oxygenated compounds and extended hydrocarbon chains through secondary reactions like Fischer–Tropsch synthesis [3]. However, DRM heavily relies on catalytic action, with noble metal-based catalysts (e.g., Pt, Rh, or Ru) exhibiting superior resistance to coke formation compared to transition metals [4–6]. Yet, their limited availability and high costs impede widespread industrial implementation [7, 8].

From an industrial standpoint, nickel emerges as a more viable active metal due to its cost-effectiveness and ample availability [8]. Ni-based catalysts encounter rapid deactivation due to carbon deposition and active site sintering [9, 10]. Recent studies have explored various supports for DRM catalysts, including mesoporous silicas [11, 12], alumina [13, 14], and zeolites [15, 16]. Moreover, nanostructured materials like TiO_2, ZnO, CeO_2, and ZrO_2 have gained attention as potential catalyst supports due to unique features such as high oxygen storage capacity and thermal stability [17, 18]. CeO_2 and ZrO_2 exhibit compelling traits, including substantial oxygen storage capacity, warranting attention in DRM applications [19].

The role of basicity emerges as a pivotal factor impacting efficiency and resistance to coke formation in these catalysts [17]. Incorporating basic promoters has shown promise in enhancing metal–support interactions, thereby augmenting Ni catalysts' activity and stability [19]. In this study, we

✉ F. Pola-Albores
francisco.pola@unicach.mx

[1] Laboratorio de Materiales y Procesos Sustentables, IIIER-Universidad de Ciencias y Artes de Chiapas, Libramiento Nte. Pte. 1150, Lajas Maciel, Tuxtla Gutiérrez, Chiapas, Mexico

[2] Laboratorio de Catálisis y Materiales, ESIQIE-Instituto Politécnico Nacional, Zacatenco, 07738 Ciudad de México, Mexico

explore the interplay between efficiency and basicity in Ni/ZrO_2 catalysts, focusing on the influence of calcium (Ca) as a promoter during the DRM reaction.

Materials and methods

Synthesis of catalyst materials

Zirconium IV oxynitrate hydrate (Sigma-Aldrich, St. Louis, MO, USA, 99 wt%), calcium nitrate tetrahydrate (Fermont-PQM, MTY, Mexico, ≥ 99 wt%), and nickel nitrate hexahydrate (Fermont-PQM, MTY, Mexico, ≥ 99 wt%), were used as sources for ZrO_2, CaO, and Ni, respectively. Sodium hydroxide (Fermont-PQM, MTY, Mexico, ≥ 97 wt%) acted as the precipitating agent. ZrO_2 and ZrO_2–CaO supports were synthesized via the co-precipitation method. In a typical synthesis, a 0.5 M Zr precursor solution underwent agitation at room temperature on a magnetic stirrer. NaOH (1 M) was slowly added to each support until reaching a pH of 11, lasting 2 h. For CaO-containing samples, a 0.1 M calcium precursor solution was added to achieve the desired calcium percentages (2% and 10%, coded as M2 and M3, respectively). Post-co-precipitation, the resulting material was washed four times with distilled water and dried at 70 °C for 15 h, followed by calcination at 700 °C for 4 h. Impregnation of supports with 15% theoretical metallic Ni was conducted using the incipient wetness impregnation method. Each support was dried for 10 h at 60 °C and then impregnated with a nickel precursor solution. The impregnated supports were placed on a magnetic stirrer at 125 °C to evaporate excess liquid. Subsequently, all three catalysts underwent calcination at 500 °C for 4 h. Samples were labeled as M1 (15% Ni/ZrO_2), M2 (2% Ca–15% Ni/ZrO_2), and M3 (10% Ca–15% Ni/ZrO_2).

Characterization techniques

The textural properties of the fresh catalyst powder were measured using a 3P Instrument Micro 100 BK100C. Powder X-ray diffraction (XRD) was employed for phase identification and quantitative analyses. Patterns were recorded on a Rigaku Ultima IV using Cu anode (K_a = 1.54187 Å) in 2θ from 20° to 100° at a scan rate of 2°/min. Temperature-programmed reduction (TPR) of catalysts was performed on a Bel Japan Belcat-B after prior treatment at 250 °C for 3 h. A reducing gas containing 5% H_2 (balanced with Ar) flowed at 50 ml/min with a heating rate of 10 °C/min. The chemical composition of samples was determined via wavelength dispersive X-ray fluorescence (WDXRF) on a Rigaku Supermini 200 equipped with a Pd anode (200 W power) coupled with RX25 and LiF (200) crystals, Zr filter, and P-10 gas flow proportional counters. FTIR measurements were conducted using a Thermo Scientific spectrophotometer model NICOLET IS50 FT-IR, operating in transmittance mode for conversion measurements with MBOH in DRIFTS within a reaction dome supported on a Praying Mantis (Harrick) with ZnSe windows. Measurements were within the range of 4000 to 700 cm^{-1} at a resolution of 4 cm^{-1} for 32 scans.

Catalytic evaluation

The DRM reaction occurred in a fixed-bed tubular reactor (I.D. = 7 mm) coupled to a gas chromatograph. Catalyst evaluation was performed at 700 °C, introducing a mixture of high-purity CH_4:CO_2 (1:1, 30 ml/min) with 80 ml/min of Ar as a diluent gas. Typically, 0.07 g of quartz wool and 0.05 g of catalyst were introduced into the tubular reactor. Reduction was conducted for 1 h at 550 °C with a flow of 80 ml/min Ar and 15 ml/min H_2. After reduction, only the Ar flow (80 ml/min) continued for 45 min. Subsequently, the temperature increased until the reaction temperature, followed by introducing CO_2 and CH_4 flows. Catalytic activity was evaluated for 24 h, and product analysis was performed using a Fuli Instruments chromatograph (GC9790II) equipped with a TCD detector and a silica-gel-packed column.

Results and discussion

The comprehensive characterization detailed in Table 1 has unveiled intriguing trends in particle size and textural properties across the synthesized catalysts. The specific surface area measurements exhibited a consistent order of M3 > M2 > M1, indicating a discernible influence of CaO content on surface characteristics. Surprisingly, the pore volume data did not mirror this trend, presenting an M2 > M1 > M3 order. Despite this divergence, all synthesized materials displayed mesoporous structures and Type IV isotherms, suggesting potential pore connectivity. These findings imply the presence of well-connected pore networks and substantial Ni dispersion, potentially countering sintering effects.

The results presented in Table 1 highlight the comparative quantitative XRD analysis with WDXRF characterization, showcasing similar calculated percentages across all three samples, particularly concerning CaO. Furthermore, Table 1 and Fig. 1 illustrate the DRIFTS results and spectra of fresh catalysts subjected to the conversion of MBOH at 70 °C, respectively. Samples M2 and M3 exhibited a characteristic band at 1670 cm^{-1}, indicative of a CO bond representing the production of acetylene groups, absent in sample M1. This distinction infers that CaO addition alters the number of basic sites on the catalyst surface. Additionally, the band at 3670 cm^{-1}, representing associated OH links characteristic

Table 1 Concentrated on microstructural, elemental, textural, and chemical properties of catalysts

Sample	ID	Crystallite size (nm)		XRF analysis (wt%)		XRD analysis (wt%)		Textural properties			Basicity (a.u.)	Formed carbon (mg)
		ZrO_2	NiO	Ni	$CaCO_3$	Ni	$CaCO_3$	Pore volume (cm^3/g)	Pore width (nm)	BET surfaces (m^2/g)		
$ZrO_2/Ni_{15\%}$	M1	9.4	20.5	22.2	–	16.6	–	0.114	13.5	24.5	68	67
$ZrO_2–Ca_{2\%}/Ni_{15\%}$	M2	9.5	23.6	22.6	1.1	17.3	1.8	0.133	10.9	29.9	2270	1767
$ZrO_2–Ca_{10\%}/Ni_{15\%}$	M3	8.3	22.5	28.0	6.9	18.4	8.53	0.087	6.6	34.6	2408	46

Carbon deposited over spent catalysts

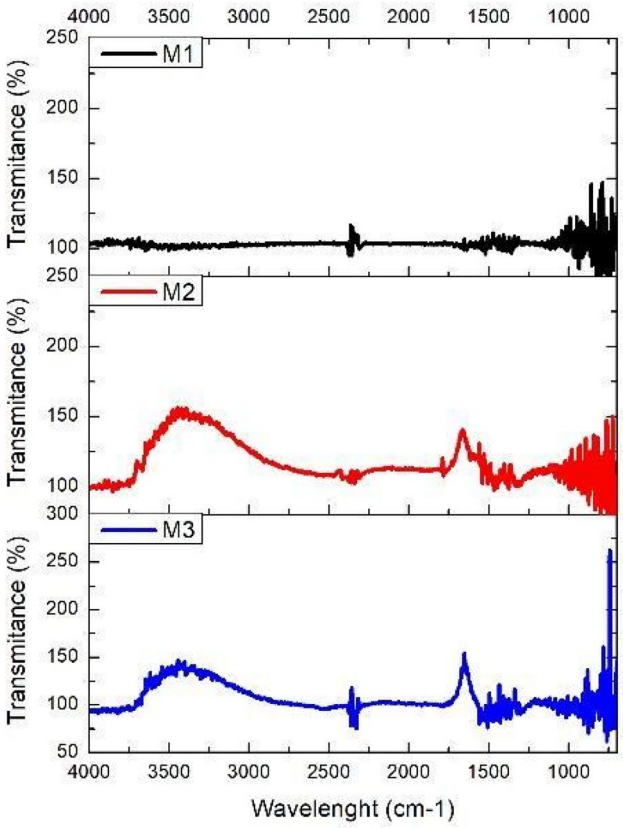

Fig. 1 DRIFT spectra in MBOH conversion

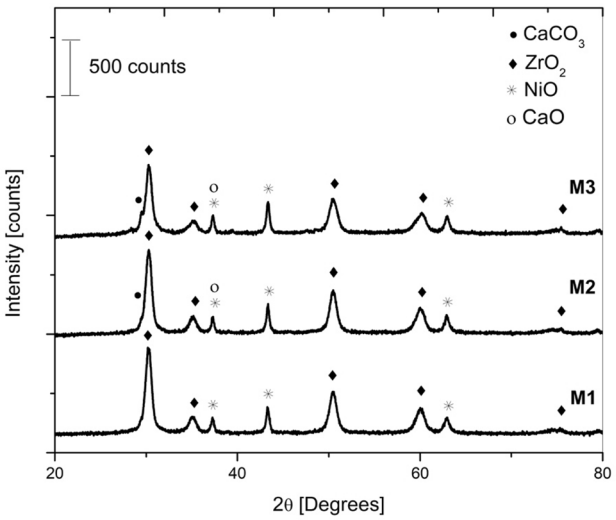

Fig. 2 X-ray diffraction patterns of fresh catalysts

of basic sites, was negligible, suggesting these links are easily eliminated. Quantifying basic sites through the area under the curve for the 1670 cm^{-1} band revealed a basicity order of M1 < M2 < M3. Consequently, it is inferred that CaO acts as a promoter-altering catalyst basicity, although the effect does not exhibit a direct proportionality to the added amount.

Figure 2 diffractogram revealed characteristic peaks attributed to ZrO_2 (PDF card 00-003-0640) and NiO (PDF card 01-078-0643) in sample M1. Additionally, samples M2 and M3 exhibited peaks corresponding to $CaCO_3$ (PDF card 01-070-0095). The crystallographic analysis determined a cubic system for ZrO_2 with lattice parameters $a = b = c = 0.51030$ nm, while NiO displayed a similar cubic crystalline system with $a = b = c = 0.41760$ nm. In contrast, $CaCO_3$ exhibited a monoclinic crystalline system with network parameters $a = 0.63340$ nm, $b = 0.49480$ nm, and $c = 0.80330$ nm. Notably, the calculated crystallite sizes from Table 1 indicated a minimal impact on the crystal size of ZrO_2 upon CaO addition. In contrast, the presence of NiO led to an estimated 18% increase in crystal size. Interestingly, the impregnated catalyst with 10 wt% CaO showcased a larger crystal size compared to its 2 wt% counterpart.

The results in Fig. 3, derived from the temperature-programmed reduction conducted with H_2, revealed notable observations upon introducing CaO into the catalysts. Specifically, an observable rightward shift in the peak corresponding to NiO reduction was noted in samples M2 and M3 upon CaO addition. A distinctive peak at 333 °C was also detected, indicating a possible mild reduction of ZrO_2, demonstrating a shift upon including CaO. Remarkably, in

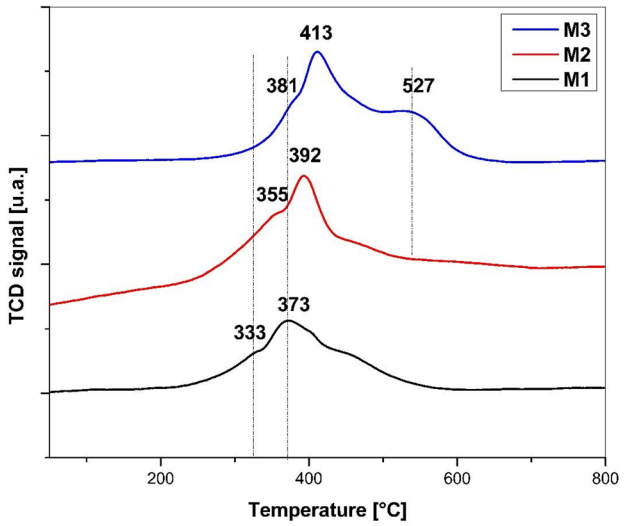

Fig. 3 H_2-TPR of calcined catalysts

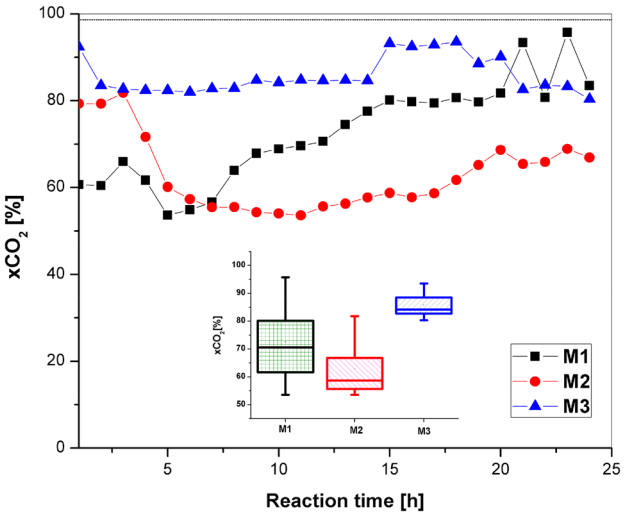

Fig. 5 CO_2 conversion profiles of evaluated catalysts

sample M3, a distinct peak at 527 °C corresponded to the reduction of CaO. However, this particular peak was absent in catalyst M2, potentially attributed to its lower CaO content (2 wt%), suggesting a correlation between the absence of this peak and the reduced percentage of CaO within the sample.

Figures 4 and 5 depict the methane and CO_2 conversion profiles observed during the DRM at 700 °C. Notably, incorporating CaO as a promoter significantly influenced the conversion and stability of the catalysts. For instance, the M3 catalyst, containing 10% CaO, exhibited markedly higher CH_4 and CO_2 conversion, demonstrating greater stability than M1. This observed enhancement can be attributed to the utilization of CaO as a promoter in the support, augmenting its basic character and consequently elevating the catalytic conversion of CO_2. Conversely, the M2 catalyst, featuring only 2% CaO, experienced deactivation, indicating that a lower percentage of CaO in the M2 sample promotes its deactivation. Moreover, the initial CH_4 conversion in the M1 sample was relatively low, progressively increasing over time. Additionally, the assessment of carbon formation during the evaluation of all catalysts is detailed in Table 1. The results confirm that excessive coke formation led to the deactivation of the M2 catalyst. In contrast, as previously highlighted, the M3 catalyst displayed the least superficial coke formation, contributing to its superior catalytic efficiency.

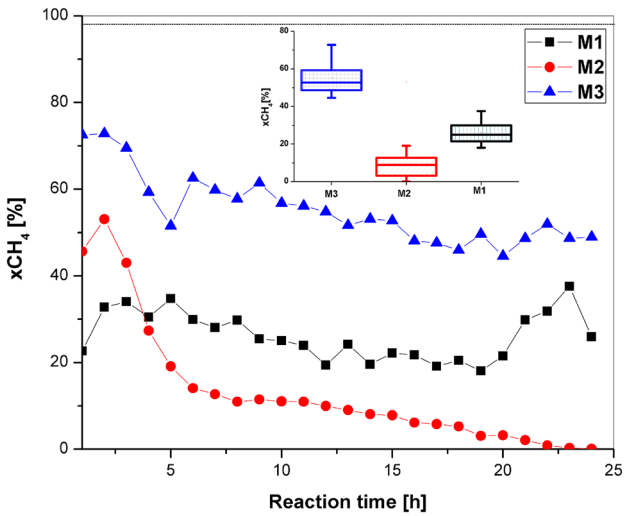

Fig. 4 CH_4 conversion profiles of evaluated catalysts

Conclusion

The introduction of CaO into Ni/ZrO_2 catalysts effectively promoted their basic character, resulting in heightened catalytic activity within the synthesized mesoporous materials, particularly enhancing the dissociation of CO_2. However, the varying percentages (2% and 10 wt%) of CaO added to the catalysts demonstrated mixed outcomes in augmenting catalytic efficiency. DRIFTS results indicated that the inclusion of CaO successfully elevated the catalysts' basicity, evident through the MBOH conversion observed in the DRIFTS spectrum. Moreover, the basicity level corresponded proportionally to the catalytic efficiency observed in the DRM evaluations. Specifically, the catalyst M3 exhibited the most extensive basic sites and displayed superior activity, followed by the M1 material, which was not promoted with CaO despite being promoted with 2 wt% CaO, the M2 catalyst, exhibited a rapid decline in methane conversions, dropping to zero after 20 h of evaluation, signifying its deactivation.

In summary, adding CaO as a promoter significantly influenced the basicity and catalytic performance of Ni/ZrO_2 catalysts. While higher CaO content notably enhanced activity, lower percentages showed inconsistent effects, emphasizing the critical role of CaO concentration in determining catalyst efficiency and stability in DRM reactions.

Author contributions The following coauthors made the following contributions to this work: VP-M: Chemical characterization (MBOH and FTIR analysis), catalyst synthesis, and evaluation. Discussion of results, data interpretation, and manuscript drafting. DS-S: XRD analysis and interpretation, and catalyst activation. Additionally, M.Sc. Santiago has contributed to gas chromatography analysis, data interpretation, image creation, formatting, and manuscript drafting. ER-V: Drafting and reviewing the work, elemental characterization via WDXRF, textural analysis, data interpretation, and discussion of results. EA: TPR characterization, data interpretation, and discussion of results; MAV: Drafting and reviewing the work, advising in the gas reaction system, catalysts evaluation, and discussion of results. FP-A: Analysis and discussion of results. Planning, coordination, and revision of all experimental details. Final formatting, correction, and approval of the version to be published.

Funding This work was completely supported by the Project SEP-CONACYT 2016-286940.

Data availability Data sharing does not apply to this article as no datasets were generated or analyzed during the current study.

Declarations

Conflict of interest On behalf of all authors, the corresponding author states that there is no conflict of interest.

References

1. N. Sun et al., Catalytic performance and characterization of Ni–CaO–ZrO_2 catalysts for dry reforming of methane. Appl. Surf. Sci. **257**(21), 9169–9176 (2011)
2. B. Jin, S. Li, X. Liang, Enhanced activity and stability of MgO-promoted Ni/Al_2O_3 catalyst for dry reforming of methane: role of MgO. Fuel **284**, 119082 (2021)
3. M. Zhang et al., Insight into the effects of the oxygen species over Ni/ZrO_2 catalyst surface on methane reforming with carbon dioxide. Appl. Catal. BCatal. B **244**, 427–437 (2019)
4. G.K. Reddy et al., Reforming of methane with carbon dioxide over $Pt/ZrO_2/SiO_2$ catalysts—effect of zirconia to silica ratio. Appl. Catal. ACatal. A **389**(1), 92–100 (2010)
5. J.F. Múnera et al., Kinetic studies of the dry reforming of methane over the Rh/La_2O_3–SiO_2 catalyst. Ind. Eng. Chem. Res. **46**(23), 7543–7549 (2007)
6. J. Niu et al., Methane dry (CO_2) reforming to syngas (H_2/CO) in catalytic process: from experimental study and DFT calculations. Int. J. Hydrog. EnergyHydrog. Energy **45**(55), 30267–30287 (2020)
7. M. Yusuf et al., Response surface optimization of syngas production from greenhouse gases via DRM over high performance Ni–W catalyst. Int. J. Hydrog. EnergyHydrog. Energy **47**(72), 31058–31071 (2022)
8. V.G. de la Cruz-Flores, A. Martinez-Hernandez, M.A. Gracia-Pinilla, Deactivation of Ni–SiO_2 catalysts that are synthetized via a modified direct synthesis method during the dry reforming of methane. Appl. Catal. ACatal. A **594**, 117455 (2020)
9. M.M. Barroso-Quiroga, A.E. Castro-Luna, Catalytic activity and effect of modifiers on Ni-based catalysts for the dry reforming of methane. Int. J. Hydrog. EnergyHydrog. Energy **35**(11), 6052–6056 (2010)
10. Y. Xu et al., A comparison of Al_2O_3 and SiO_2 supported Ni-based catalysts in their performance for the dry reforming of methane. J. Fuel Chem. Technol. **47**(2), 199–208 (2019)
11 X.Y. Gao, K. Hidajat, S. Kawi, Facile synthesis of Ni/SiO_2 catalyst by sequential hydrogen/air treatment: a superior anti-coking catalyst for dry reforming of methane. J. CO2 Util. **15**, 146–153 (2016)
12. J.G. Roblero et al., Ni and Ni_3C catalysts supported on mesoporous silica for dry reforming of methane. Int. J. Hydrog. EnergyHydrog. Energy **44**(21), 10473–10483 (2019)
13. P.K. Chaudhary, N. Koshta, G. Deo, Effect of O_2 and temperature on the catalytic performance of Ni/Al_2O_3 and $Ni/MgAl_2O_4$ for the dry reforming of methane (DRM). Int. J. Hydrog. EnergyHydrog. Energy **45**(7), 4490–4500 (2020)
14. Z. Bian et al., Dry reforming of methane on Ni/mesoporous-Al_2O_3 catalysts: effect of calcination temperature. Int. J. Hydrog. EnergyHydrog. Energy **46**(60), 31041–31053 (2021)
15. A.J. Najfach, C.B. Almquist, R.E. Edelmann, Effect of manganese and zeolite composition on zeolite-supported Ni-catalysts for dry reforming of methane. Cataly. Today **369**, 31–47 (2021)
16 S. Kweon et al., Nitrided Ni/N-zeolites as efficient catalysts for the dry reforming of methane. J. CO2 Util. **46**, 101478 (2021)
17. A.S.A.-F. Muhammad AwaisNaeem, W.U. Khan, A.E. Abasaeed, A.H. Fakeeha, Syngas production from dry reforming of methane over nano Ni polyol catalysts. Int. J. Chem. Eng. Appl. **4**(5), 315–320 (2013)
18. R. Zhou et al., Facile synthesis of multi-layered nanostructured Ni/CeO_2 catalyst plus in situ pre-treatment for efficient dry reforming of methane. Appl. Catal. BCatal. B **316**, 121696 (2022)
19. M. Rezaei et al., CO_2 reforming of CH_4 over nanocrystalline zirconia-supported nickel catalysts. Appl. Catal. BCatal. B **77**(3), 346–354 (2008)